Microphysics Regime Impacts on the Relationship between Orographic Rain and Orographic Forcing in the Coastal Mountains of Northern California

DAVID E. KINGSMILL

Cooperative Institute for Research in Environmental Sciences, University of Colorado Boulder, Boulder, Colorado

PAUL J. NEIMAN AND ALLEN B. WHITE

NOAA/Earth System Research Laboratory, Boulder, Colorado

(Manuscript received 27 April 2016, in final form 5 August 2016)

ABSTRACT

This study examines the impact of microphysics regime on the relationship between orographic forcing and orographic rain in the coastal mountains of Northern California using >4000 h of data from profiling Doppler radars, rain gauges, and a GPS receiver collected over 10 cool seasons. Orographic forcing is documented by hourly upslope flow, integrated water vapor (IWV), and IWV flux observed along the coast at Bodega Bay (BBY; 15 m MSL). Microphysics regime is inferred in the coastal mountains at Cazadero (CZC; 478 m MSL), where hourly periods of brightband (BB) and nonbrightband (NBB) rain are designated. BB rain is associated with a microphysics regime dominated by the seeder–feeder process while NBB rain is associated with a microphysics regime dominated by the warm-rain process. Mean BBY upslope flow, IWV, and IWV flux are ~16%, ~5%, and ~19% larger, respectively, for NBB rain compared to BB rain, while mean CZC rain rate is ~33% larger for BB rain compared to NBB rain. The orographic enhancement ratio of CZC to BBY rain rate is 3.7 during NBB rain and 2.7 during BB rain. Rain rate at CZC increases as orographic forcing at BBY increases. For a given amount of BBY orographic forcing, mean CZC rain rates are larger for BB rain compared to NBB rain. Correlation coefficients associated with the relationship between CZC rain rate and BBY orographic forcing are smaller for NBB rain relative to BB rain, but these differences are not statistically significant.

1. Introduction

Cool-season precipitation in the western United States is strongly modulated by the regions' complex terrain. Narrow corridors of concentrated horizontal water vapor transport within landfalling extratropical cyclones called atmospheric rivers (ARs; Zhu and Newell 1998; Ralph et al. 2004) impact the terrain and the associated orographic lift leads to enhanced precipitation. Considerable attention has been given to orographic precipitation enhancement for the larger inland mountain ranges of the west (>3 km MSL tall and >500 km long), such as the Cascades in Washington and Oregon (e.g., Hobbs 1975; Stoelinga et al. 2003; Medina et al. 2007) and the Sierra Nevada in California (e.g., Reynolds and Dennis 1986; Dettinger et al. 2004; Neiman et al. 2013). Smaller terrain along the coastline (typically <1.5 km MSL tall and <100 km long) can also significantly enhance precipitation (e.g., Elliott and Hovind 1964; Ralph et al. 2003, 2013b). In fact, precipitation in these orographic locales unimpeded by upstream topography can lead to severe flooding that incurs millions of dollars in property damage (e.g., NOAA 1982, 1998; Smith et al. 2005). One factor that contributes to flood risk in the smaller terrain of the coastal mountains is that most of the precipitation falls in the form of rain rather than snow, which leads to rapid runoff. Another factor is the relative sparsity of dams in the coastal mountains compared to the Cascades and Sierra Nevada, which provides minimal capacity to control the runoff.

The amount of orographically enhanced precipitation is dependent on the magnitude of moist airflow ascending the windward slope of a mountain barrier (i.e., upslope flow). This dependence has been demonstrated in several modeling (e.g., Collier 1975; Rhea 1978;

Corresponding author address: David E. Kingsmill, CIRES, University of Colorado Boulder, UCB 311, Boulder, CO 80309.
E-mail: david.kingsmill@colorado.edu

DOI: 10.1175/JHM-D-16-0103.1

Sinclair 1994) and observational (e.g., Nordø and Hjortnæs 1966; Hill et al. 1981; Neiman et al. 2002) investigations. Of these studies, Neiman et al. (2002) have provided the most comprehensive depiction of the relationship to date by utilizing data collected over an entire cool season at three couplets of instrumented sites along the California coastline. Each couplet was composed of a wind profiler at the coast and a precipitation gauge downstream in the adjacent coastal mountains characterized by mean crest heights of 0.7–1.1 km. They examined significant precipitation events defined by rainfall in the coastal mountains that exceeded 12.5 mm accumulation and 8 h duration. The northern, central, and southern couplets of their study included 25, 20, and 9 significant events spanning 468, 362, and 145 h, respectively. Time series of hourly and 500-m-vertical-layer-averaged upslope flow[1] derived at each vertical bin of the wind profiler (100-m spacing) were fitted in a linear, least squares sense against corresponding time series of hourly rain rate in the downstream coastal mountains. The regression analyses for the entire cool season produced vertical profiles of correlation coefficient with maximum values of 0.5–0.7 at ~1 km MSL. This level is close to or slightly above the mean barrier crest height of the coastal terrain. The height of the correlation maximum also coincides with the typical height of prefrontal low-level jets observed offshore of California (Ralph et al. 2005).

Neiman et al. (2009) advanced the analysis by incorporating GPS-derived, column-integrated water vapor (IWV) information at the northern couplet (Bodega Bay at the coast and Cazadero in the downstream coastal mountains) for a period that extended over four cool seasons but was not based only on significant precipitation events. Upslope flow at each vertical bin of the Bodega Bay (BBY) wind profiler was multiplied by IWV from the collocated GPS receiver to derive the bulk upslope IWV flux, or simply the IWV flux. Because water vapor is typically concentrated in the lower troposphere, the IWV flux is a first-order estimate of low-level water vapor flux. Linear regressions of hourly, 300-m-layer-averaged upslope flow and IWV flux from BBY with hourly rain rate from Cazadero (CZC) for the four-season composite produced vertical profiles of correlation coefficient with maximum values of 0.62 for upslope flow and 0.68 for IWV flux, both at ~1 km MSL. Thus, an additional ~7% of the rain-rate variation at CZC was explained with IWV flux compared to upslope flow alone.

As Neiman et al. (2002, 2009) have documented, there is a noticeable dependence of orographic rainfall on orographic forcing (i.e., upslope flow and IWV flux). However, the relationship is far from perfect since maximum correlation coefficients for single- or multi-season composites are less than 0.7. One source of uncertainty in the relationship may be related to transient mesoscale features such as fronts and jet streaks that can produce updrafts whose magnitudes approach the magnitude of orographically forced updrafts. Perhaps the largest potential source of uncertainty in the relationship is linked to cloud and precipitation microphysics. A given amount of orographic forcing may lead to different orographic rainfall rates depending on microphysics regime, defined here as the dominant microphysical process in effect. One microphysics regime is dominated by the well-known seeder–feeder process that occurs with relatively deep clouds where water drops in the low-level, orographically forced feeder cloud are accreted or collected by larger ice or liquid hydrometeors, respectively, emanating from seeder clouds aloft (Bergeron 1965). Seeder clouds may not be entirely distinct from feeder clouds (Browning 1980) and often originate from the same extratropical frontal systems that force orographic feeder clouds. Another microphysics regime is dominated by the warm-rain (i.e., collision–coalescence) process that occurs with relatively shallow feeder clouds unaccompanied by significant seeder clouds aloft (White et al. 2003; Neiman et al. 2005; Kingsmill et al. 2006). This regime produces larger numbers of smaller raindrops compared to precipitation generated by the seeder–feeder process (Martner et al. 2008).

The impact of microphysics regime on the relationship between orographic rain and orographic forcing was briefly addressed by White et al. (2003). They examined 33 significant precipitation events at CZC during a single cool season spanning a total of 602 h using the same criteria as Neiman et al. (2002). White et al. (2003) documented how the relationship between rain rate and upslope flow at CZC during warm-rain periods was characterized by a correlation coefficient of 0.74, ~40% larger than the correlation coefficient for the 33-event composite as a whole of 0.52. However, they did not examine the relationship for specific seeder–feeder periods. They also did not quantify how the slope of the linear relationship varied as a function of microphysics regime. Additionally, White et al. (2003) were not able to incorporate water vapor into the analysis of orographic forcing since GPS IWV information was not available at the time. Finally, their single-season analysis only included 38 hourly data points of upslope flow versus rain rate during warm-rain

[1] All references to upslope flow in this paper, whether associated with this or other studies, are synonymous with cross-barrier-component flow.

conditions, which diminishes the statistical significance of the results. In fact, White et al. (2003) acknowledged that a comparable multiseason analysis was required to validate the generality of their findings.

The present study addresses these limitations through analysis of data from profiling Doppler radars, rain gauges, and a GPS receiver collected over 10 cool seasons at CZC and BBY. More than 4000 h of data from these instruments are examined when accumulating rain is observed at CZC and 1495 h when CZC rain rates exceeded 1 mm h^{-1}. For the latter, 910 h occurred during seeder–feeder conditions and 585 h during warm-rain conditions. This study is unique because it explores the impact of microphysics regime on the relationship between orographic forcing and orographic rain with an approach that employs a large data sample that includes water vapor information. Section 2 describes the observing systems utilized in the analysis and how data were processed. The relationship between orographic forcing, orographic rain, and microphysics regime is illustrated in section 3 using a significant 3-day precipitation event as a case study example. Section 4 examines the relationship for all 10 seasons using a composite analysis. Finally, a summary of the analysis and the resulting conclusions from the study are presented in section 5.

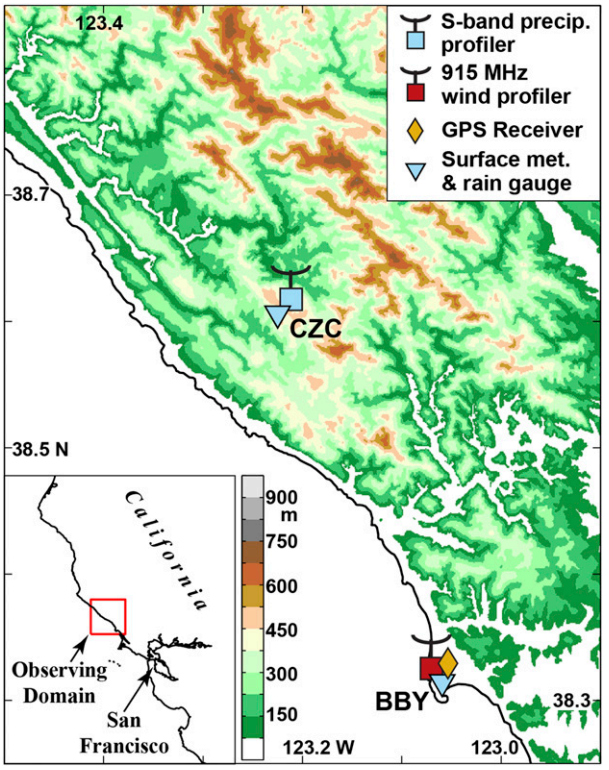

FIG. 1. Topographic map of study domain. The type and location of observing systems are indicated by symbols defined in the legend. Inset map shows position of study domain relative to the state of California. Color scale for terrain height is to the right of inset map.

2. Observing systems and data processing

The data used in this study were collected along the coast and in the adjacent coastal mountains north of San Francisco, California (Fig. 1), as part of the Pacific Land-Falling Jets (PACJET) and Hydrometeorology Testbed (HMT) experiments (Ralph et al. 2013a) operated by the National Oceanic and Atmospheric Administration (NOAA)/Earth System Research Laboratory (ESRL). Portions of 10 cool seasons are included in the analysis starting in 2001 and ending in 2012, with a two-season deployment break from 2001/02 to 2002/03 (Table 1). The number of days with data varies from 48 during the 2000/01 season to 171 during the 2009/10 season and totals 1167.

One of the primary observing systems was a 915-MHz Doppler wind profiler (Ecklund et al. 1988; Carter et al. 1995) deployed at BBY. The wind profiler provided hourly averaged vertical profiles of horizontal wind velocity from ~0.1 km MSL up to ~4–6 km MSL[2] with ~100-m vertical resolution. Data were edited with the vertical/temporal continuity method described by Weber et al. (1993). A dual-channel GPS receiver was also deployed at BBY allowing retrieval of IWV at 30-min intervals (Duan et al. 1996; Mattioli et al. 2007). Hourly averages of IWV were derived to facilitate integration with the wind profiler data. Another key observing system employed in this study was an S-band (3 GHz) precipitation profiler (S-PROF) (White et al. 2000) deployed at CZC. This profiler provided vertical profiles of reflectivity and Doppler vertical velocity from ~0.7 km MSL up to ~8–10 km MSL[2] with ~60-m vertical resolution at 30–120-s intervals.[2] Finally, 2-min-resolution surface observations of temperature, relative humidity, pressure, horizontal winds, and rainfall were collected at both BBY and CZC. Rainfall was measured with a tipping-bucket gauge having 0.01-in. (0.25 mm) precision.

Microphysical context for the relationship between orographic forcing at BBY and orographic rainfall at CZC was inferred from S-PROF data using a variant of the rainfall process partitioning algorithm (RPPA) developed by White et al. (2003). The RPPA from White et al. (2003) inspected 30-min periods of CZC S-PROF data occurring with surface rain rate exceeding 1 mm h^{-1}. Individual S-PROF profiles of reflectivity and Doppler vertical velocity from these periods were examined to

[2] Season-dependent variation.

TABLE 1. Date ranges and number of days with data at CZC and BBY for each of the 10 cool seasons included in the analysis. Rainfall characteristics at CZC and BBY are provided for each season. Time at CZC represents the number of hours when measurable rain (i.e., ≥0.25 mm) was observed. Rate at BBY is based on rain time at CZC; no-rain time at BBY represents the subset of CZC rain time when no rain is observed at BBY. Rainfall ratio is the CZC rain rate divided by the BBY rain rate. The 10-season totals for number of days with data, rainfall accumulations, CZC rain time, and BBY no-rain time are shown at the bottom. Rain rates and rainfall ratio in this row are based on total accumulations and total CZC rain time.

Cool season		CZC rainfall			BBY rainfall			CZC/BBY rainfall ratio
Date	Number of days	Rain time (h)	Accumulation (mm)	Rate (mm h^{-1})	Accumulation (mm)	Rate (mm h^{-1})	No-rain time (h)	
From 12 Jan to 8 Mar 2001	48	275	618	2.3	228	0.8	130	2.7
From 22 Dec 2003 to 21 Mar 2004	84	296	756	2.6	331	1.1	115	2.3
From 28 Dec 2004 to 31 Mar 2005	78	345	430	1.3	320	0.9	131	1.3
From 16 Nov 2005 to 25 Apr 2006	120	631	1739	2.8	697	1.1	249	2.5
From 1 Dec 2006 to 30 Apr 2007	143	391	856	2.2	277	0.7	176	3.1
From 21 Nov 2007 to 9 Apr 2008	126	376	1098	2.9	273	0.7	198	4.0
From 8 Nov 2008 to 11 May 2009	145	465	983	2.1	202	0.4	263	4.9
From 7 Nov 2009 to 11 May 2010	171	538	1421	2.6	371	0.7	284	3.8
From 3 Nov 2010 to 31 Mar 2011	126	463	975	2.1	402	0.9	224	2.4
From 16 Nov 2011 to 21 Mar 2012	126	278	636	2.3	194	0.7	122	3.3
Total	1167	4058	9512	2.3	3295	0.8	1892	2.9

determine the existence of a radar bright band using the technique described by White et al. (2002). If 50% or more of the individual profiles within a 30-min period contained a bright band, rainfall was ascribed to the brightband (BB) rain category. White et al. (2003) classified a subcategory of BB rain called hybrid rain when reflectivity increased below the bottom of the bright band with a slope $\leq -0.1\,\mathrm{dB}Z_e\,\mathrm{km}^{-1}$. They found that ~75% of BB rain accumulation occurred with hybrid rain. If fewer than 50% of the individual profiles within a 30-min period contained a bright band, rainfall was ascribed to the nonbrightband (NBB) rain category unless a visual inspection of the data indicated the presence of convection where a bright band might be obscured. This visual inspection involved subjective examination of S-PROF reflectivity and Doppler velocity data in time–height form along with concurrent wind profiler and surface meteorology datasets to provide context. BB rain is associated with a microphysics regime primarily representative of the seeder–feeder process while NBB rain is associated with a microphysics regime primarily representative of the warm-rain process.

The RPPA employed in this study differed from White et al. (2003) primarily because of the use of a 60-min averaging period that was selected to facilitate integration with the orographic-forcing data. Additionally, hybrid rain was not classified as a subcategory of BB rain because the vast majority of BB rain is hybrid rain and the fact that the $-0.1\,\mathrm{dB}Z_e\,\mathrm{km}^{-1}$ slope threshold is somewhat arbitrary. Martner et al. (2008) also employed this approach. Other aspects of the RPPA were the same, such as the >1 mm h^{-1} rain-rate threshold and the requirement that ≥50% (<50%) of the individual profiles during the averaging period contain a bright band for designation of BB (NBB) rain.

3. Case study example: 14–16 February 2011

A significant precipitation event that impacted Northern California on 14–16 February 2011 is now described as a means to illustrate the relationship between orographic forcing, orographic rain, and microphysics regime. This case has been documented in detail by Kingsmill et al. (2013). The landfalling winter storm associated with this event produced two distinct episodes of rainfall at BBY and CZC (Fig. 2): episode 1 from ~0600 UTC 14 February to ~0600 UTC 15 February and episode 2 from ~0600 UTC 15 February to ~1800 UTC 16 February. Hourly rain rates at CZC were consistently larger than those at BBY during episode

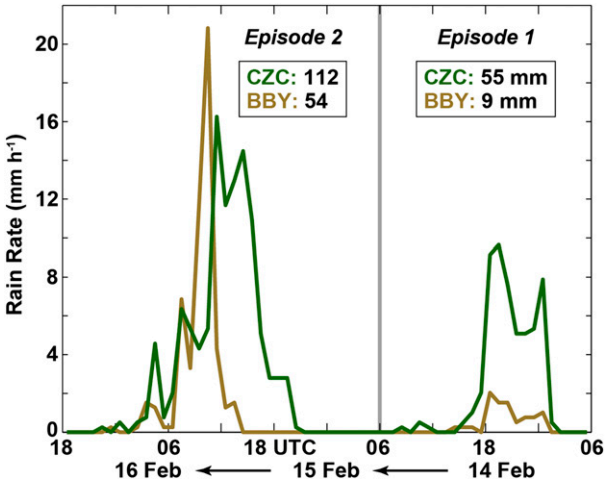

FIG. 2. Time series of hourly rain rate from the tipping-bucket rain gauges at CZC (green) and BBY (gold) for the 14–16 Feb 2011 precipitation event. Time increases from right to left to portray the advection of synoptic features from west to east. The boundary between episodes 1 and 2 is indicated by the thick gray vertical line. Total rainfall accumulations at each site are shown for each episode.

1, with associated rainfall accumulations of 55 and 9 mm at CZC and BBY, respectively. This represents a CZC/BBY orographic enhancement factor of 6.1. In contrast, hourly rain rates at CZC and BBY were more variable with respect to each other during episode 2, with values at CZC larger, smaller, and about the same as those at BBY depending on the time. Despite this variability, the rainfall accumulation at CZC of 112 mm still exceeded the rainfall accumulation at BBY of 54 mm, but only by a factor of 2.1. Overall, accumulations and peak rain rates were larger during episode 2 compared to episode 1.

Precipitating clouds over CZC were relatively shallow during episode 1, with tops often below 3 km MSL and rarely above 4 km MSL (Fig. 3). While brightband signatures were occasionally detected between 1.5 and 2.0 km MSL, NBB rain was the dominant rainfall type over this period. It is hypothesized that radar echoes above 2 km MSL were produced by a combination of small supercooled rain drops and ice crystals mostly unable to elicit a brightband signature. In contrast, during episode 2, precipitating clouds usually extended above 3 km MSL and tops often reached 4–6 km MSL. Given the deeper layer of clouds above 2 km MSL capable of forming relatively large ice crystal aggregates, it is not surprising that brightband signatures were more prevalent during this period and that BB rain was the dominant rainfall type. The four hours of NBB rain classified during episode 2 occurred in connection with perceptible bright bands. However, bright bands were detected in less than 50% of the profiles during each of those hours, prompting the designation of NBB rain.

Synoptic forcing for the precipitation event occurred in association with the Northern California landfall of two ARs, one for each of the two rainfall episodes at CZC and BBY. The first AR (AR1) made landfall during episode 1 with a 180°–360° orientation and occurred in connection with a transient short-wave trough offshore of Northern California embedded in a broad cyclonic circulation at 500 hPa centered over the Gulf of Alaska [Figs. 2a–c of Kingsmill et al. (2013)]. The second AR (AR2) made landfall during episode 2 with a 230°–50° orientation as the parent Gulf of Alaska cyclone progressed eastward toward the coast of British Columbia [Figs. 2d–f of Kingsmill et al. (2013)]. Relatively strong southerly to southwesterly winds associated with both ARs are evident above BBY (Fig. 4), with local maxima of AR-parallel wind speed centered at ~1 km MSL. These features are consistent with the structure of prefrontal low-level jets. Notably, there is no evidence of low-level blocked flow as was often observed by Neiman et al. (2002).

Orographic forcing for this event was diagnosed by deriving mean upslope flow in the 300-m vertical layer above BBY centered at 1 km MSL. The upslope component for the coastal mountains surrounding CZC is directed toward 50° based on the mean ridge orientation for the area. Neiman et al. (2009) observed that BBY upslope flow derived in the 850–1150 m MSL layer produced the largest correlation coefficients with rain rate at CZC. Distinct maxima of upslope flow in this layer are evident during the passage of both ARs (Fig. 5a), with values slightly larger for AR2 (~22 m s^{-1}) compared to AR1 (~20 m s^{-1}). GPS-derived IWV data from BBY provide additional orographic-forcing context (Fig. 5b). Like upslope flow, there are distinct maxima of IWV during the passage of both ARs. However, the IWV maxima are about the same for both ARs (~2.2 cm) and they lag the upslope maxima by ~2–4 h. Mean upslope flow and IWV at BBY were multiplied to derive the IWV flux (Fig. 5c), which exhibits an evolution that is more similar to upslope flow than IWV. Peak values of upslope flow, IWV, and IWV flux in both ARs exceeded 12.5 m s^{-1}, 2 cm, and 25 cm m s^{-1}, respectively, the thresholds for AR conditions as defined by Neiman et al. (2009).

There is a clear relationship between rain rate at CZC and 850–1150 m MSL mean upslope flow above BBY for the 34 hourly data points encompassing both episodes of rainfall (Fig. 6a); CZC rain rate increases as a function of increasing BBY upslope flow. A least squares linear fit of the data produces a correlation coefficient r of 0.82. The relationship between CZC rain rate and BBY IWV is less robust, with a relatively wide range of rain rates

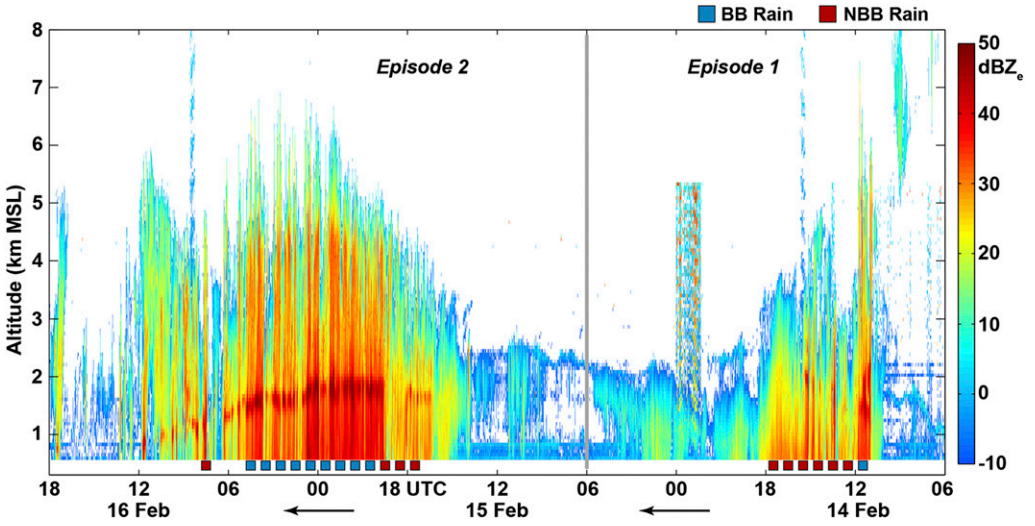

FIG. 3. Time–height cross section of reflectivity from the S-PROF at CZC for the 14–16 Feb 2011 precipitation event. Time increases from right to left to portray the advection of synoptic features from west to east. The boundary between episodes 1 and 2 is indicated by the thick gray vertical line. BB and NBB rain type is indicated by the blue- and red-filled squares, respectively, located above the lower horizontal axis. Color scale for reflectivity is shown on the right.

at IWV values exceeding 2 cm (Fig. 6b). Not surprisingly, r is only 0.64. The relationship between CZC rain rate and BBY IWV flux (Fig. 6c) is slightly better correlated ($r = 0.86$) than the relationship between CZC rain rate and BBY upslope flow, a result consistent with the findings of Neiman et al. (2009). Given the relatively small sample size, the differences between these correlation coefficients may not be significant since the associated 95% confidence intervals (CI_{95}) exhibit considerable overlap.

The relationship between orographic forcing at BBY and orographic rainfall at CZC exhibits variability that depends on CZC rainfall type, which is a proxy for dominant microphysics regime (i.e., seeder–feeder process for BB rain and warm-rain process for NBB rain). Hourly samples associated with BB rain show a tendency

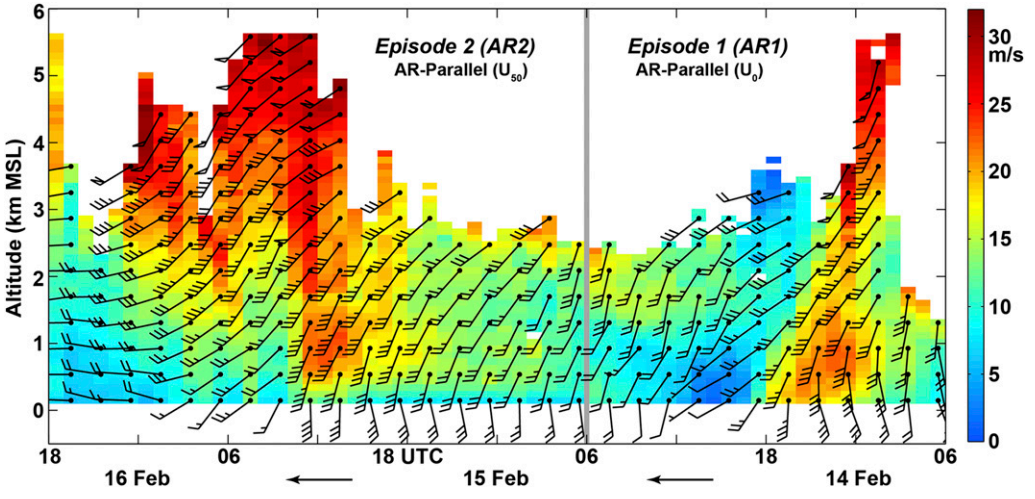

FIG. 4. Time–height cross section of horizontal wind speed and direction from the wind profiler at BBY for the 14–16 Feb 2011 precipitation event. Flags, full barbs, and half barbs equal 25, 5, and 2.5 m s^{-1}, respectively. Time increases from right to left to portray the advection of synoptic features from west to east. The boundary between episodes 1 and 2 is indicated by the thick gray vertical line. AR-parallel-component wind speed (toward 0° for episode 1 and toward 50° for episode 2) is shown by the colored pixels with values scaled as shown on the right.

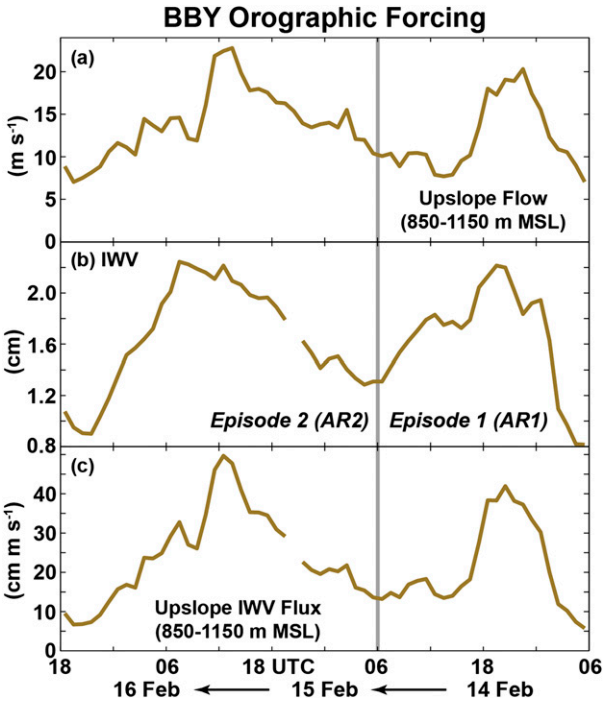

FIG. 5. Time series of orographic forcing from the wind profiler and GPS receiver at BBY for the 14–16 Feb 2011 precipitation event: (a) mean upslope flow in the 850–1150 m MSL layer, (b) IWV, and (c) upslope IWV flux. Time increases from right to left to portray the advection of synoptic features from west to east. The boundary between episodes 1 and 2 is indicated by the thick gray vertical line.

to have larger rain rate for a given amount of forcing compared to NBB rain. Unfortunately, the relatively small number of hourly BB (10) and NBB (10) rain samples for this case does not allow separate statistically significant linear fits for each population to quantify the impact of rainfall type, and by extension microphysics regime, on the relationship between orographic forcing and orographic rainfall. The composite analysis that follows will address this limitation.

4. Composite analysis

a. Independent of microphysics regime

As a means to provide context relative to the Neiman et al. (2009) four-season composite, it is important to first examine the relationship of orographic rain to orographic forcing independent of microphysics regime for the 10-season composite of this study. A summary of rainfall statistics at CZC and BBY for the 10-season composite is shown in Table 1. These statistics are derived from hourly samples that satisfy the following joint criteria: nonmissing data from the wind profiler, GPS receiver, and rain gauge at BBY; nonmissing data from the rain gauge at CZC; and at least 0.25 mm of rainfall accumulation at CZC. This composite is not based on significant precipitation events and does not require the existence of AR conditions as defined by Neiman et al. (2009). A total of 9512 mm of rain accumulated at CZC over a period of 4058 h for the 10-season composite. This corresponds to a mean rain rate of 2.3 mm h^{-1}, which is the same value observed at CZC in the four-season composite described by Neiman et al. (2009). Seasonal total rainfall accumulations varied from 430 mm during 2004/05 to 1739 mm during 2005/06. Seasonal mean rain rates were also lowest during 2004/05 (1.3 mm h^{-1}) but were slightly larger during 2007/08 (2.9 mm h^{-1}) compared to 2005/06 (2.8 mm h^{-1}).

The 10-season composite rainfall accumulation and mean rain rate at CZC were almost a factor of 3 larger than those observed at BBY (3295 mm and 0.8 mm h^{-1}, respectively), a difference that can be attributed to

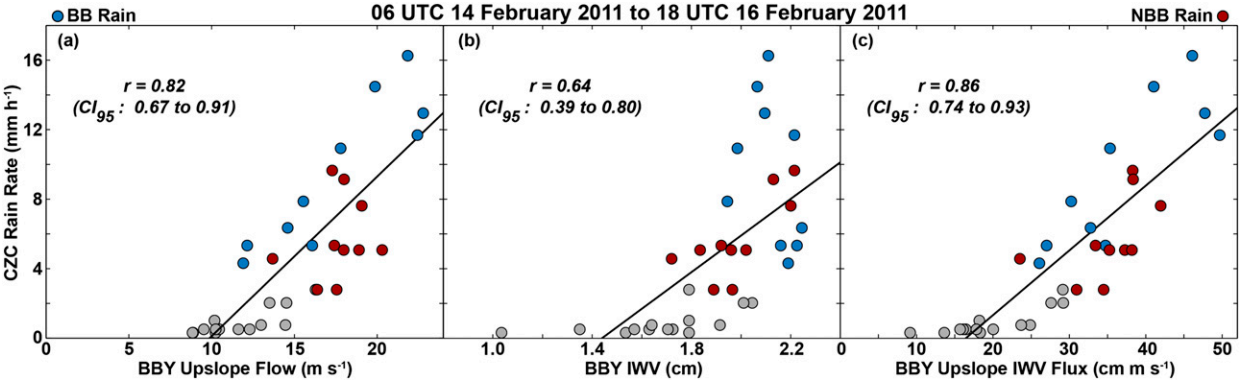

FIG. 6. Scatter of hourly (a) upslope flow, (b) IWV, and (c) upslope IWV flux at BBY vs hourly rain rate at CZC for the 14–16 Feb 2011 precipitation event. The linear fit, correlation coefficient (i.e., r), and associated CI_{95} of the correlation coefficient are shown for each set of points. BB and NBB rain type is indicated by the blue- and red-filled circles, respectively. Gray-filled circles represent hours where neither BB nor NBB rain was designated.

orographic enhancement in the coastal mountains. In contrast, Neiman et al. (2009) observed a CZC/BBY orographic enhancement factor of ~2 in their study. The orographic enhancement in the present study produced accumulating rainfall at CZC with no rainfall at BBY for a little less than half of the hourly samples in the composite. Like CZC, the maximum seasonal total accumulation at BBY (697 mm) occurred during 2005/06. However, the minimum seasonal total accumulation at BBY (194 mm) occurred during 2011/12, which differs from the season when that metric was observed at CZC. Seasonal CZC/BBY rainfall ratios varied from 1.3 during 2004/05 to 4.9 during 2008/09, a relatively wide range of variation compared to the four-season composite of Neiman et al. (2009).

While the most common values of hourly rain rate at CZC were between 0 and 1 mm h^{-1}, values slightly exceeding 20 mm h^{-1} were observed (Fig. 7a). The distribution of hourly rain rates at BBY was narrower (Fig. 7b), although a few 1-h outliers exist at rates exceeding 16 mm h^{-1} (e.g., see also Fig. 2). Note that the BBY histogram of hourly rain rate does not include the 1892 samples with a value of zero.

The distribution of BBY orographic forcing for the 10-season composite is Gaussian in nature (Fig. 8). This population of data is derived from the same criteria used to construct Table 1. As shown in Fig. 8a, values of 850–1150 m MSL mean upslope flow (hereafter referred to simply as upslope flow) extend from −12.1 to 36.1 m s^{-1} with a mean μ of 9.0 m s^{-1} that approximately coincides with the mode of the distribution. Values of IWV extend from 0.5 to 4.5 cm with a μ of 2.0 cm (Fig. 8b). The mode of the IWV distribution was relatively wide and less distinct than the mode for the upslope flow distribution.

The distributions of upslope flow and IWV are related to each other but r is only 0.42 (Fig. 9), which is relatively poor compared to the r of 0.64 observed by Neiman et al. (2009). While the scatter is significant, larger values of upslope flow are generally observed with larger values of IWV. This provides some context for interpretation of the IWV-flux distribution (Fig. 8c), whose values extend from −24.8 to 109.5 cm m s^{-1} with a μ of 19.4 cm m s^{-1}. In relative terms, the IWV-flux distribution is wider and skewed to larger values than the upslope-flow and IWV distributions.

Hourly rain rate at CZC increases as orographic forcing at BBY increases. This is evident in the color-coded scatter of upslope flow versus IWV (Fig. 9). Rain rates exceeding 10 mm h^{-1} occurred 91% of the time when upslope flow exceeded 12.5 m s^{-1} and IWV exceeded 2 cm, the thresholds for AR conditions. This result closely matches the 94% probability of detection observed by Neiman et al. (2009). However, the 10 mm h^{-1} rain-rate exceedance only occurred 18% of the time when both of these orographic-forcing thresholds were exceeded, a false alarm ratio of 82%.

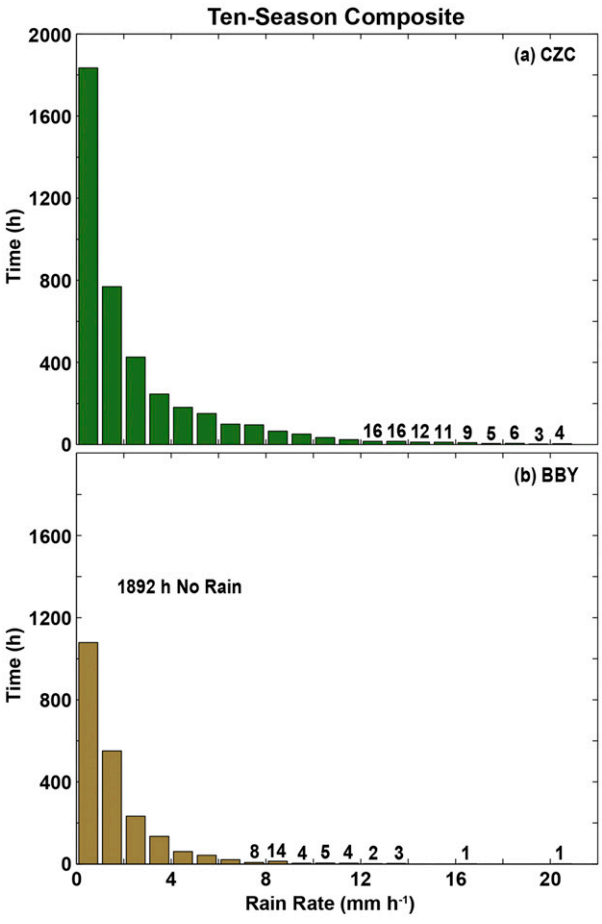

FIG. 7. Histograms of hourly rain rate at (a) CZC and (b) BBY for the 10-season composite. Rain-rate bins of 1 mm h^{-1} are used. The number of hours is shown above bars having less than 20 h of data.

The relationship is also apparent when viewing the joint distribution of CZC rain rate versus BBY orographic forcing as represented by the number of hourly samples in each joint rain-rate and orographic-forcing bin (Fig. 10). This population of hourly samples is ~4% smaller (3887) than the total of 4058 h since it incorporates the additional constraint of upslope flow greater than zero. The correlation coefficients for the unbinned scatter of CZC rain rate versus BBY upslope flow (Fig. 10a), IWV (Fig. 10b), and IWV flux (Fig. 10c) are 0.63, 0.41, and 0.67, respectively. These values compare very well with the corresponding values of 0.62, 0.45, and 0.68 observed by Neiman et al. (2009), including the slightly improved correlation with IWV flux relative to the correlation with upslope flow. The difference between upslope-flow and IWV-flux correlation coefficients in the present study is

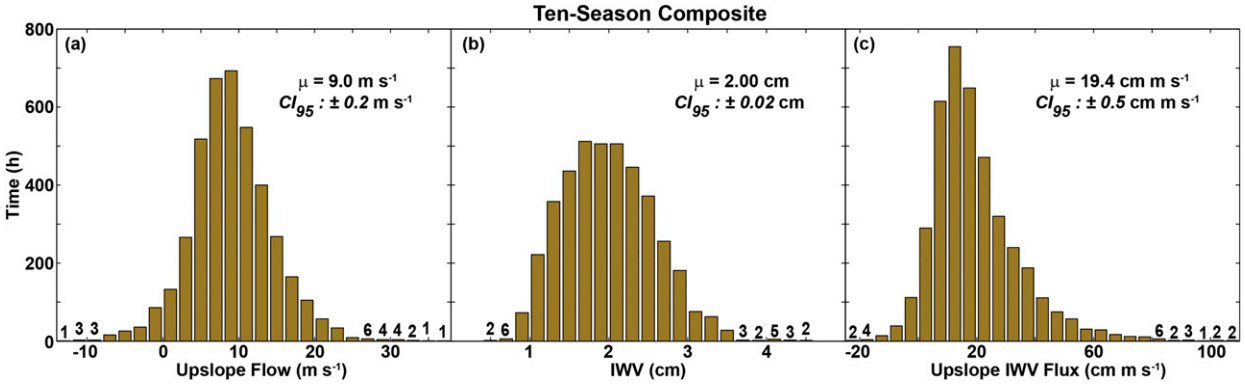

FIG. 8. Histograms of hourly (a) upslope flow (bins of 2 m s^{-1}), (b) IWV (bins of 0.2 cm), and (c) upslope IWV flux (bins of 5 cm m s^{-1}) at BBY for the 10-season composite. The mean (i.e., μ) and CI_{95} of the mean for each distribution is indicated. The number of hours is shown above bars having less than 8 h of data.

significant at the 95% confidence level since their respective CI_{95} do not overlap.

An alternative illustration of the relationship is provided by examining average values of CZC rain rate in BBY orographic-forcing bins (Fig. 11). Average CZC rain rate clearly increases as orographic forcing increases. Over the range of observed orographic forcing, average CZC rain rate increases more with upslope flow (Fig. 11a) than IWV (Fig. 11b), but more than either with IWV flux (Fig. 11c). The rate of average CZC rain-rate increase is not constant as a function of orographic forcing. Average CZC rain rate increases more rapidly when upslope flow, IWV, and IWV flux exceed ~10 m s^{-1}, ~2.5 cm, and 20 cm m s^{-1}, respectively.

Interestingly, average BBY rain rate also increases as orographic forcing increases, but by a smaller amount than average CZC rain rate. Given that BBY is located upstream of the coastal mountains, this trend is not likely associated with orographic enhancement. Rather, the trend may be linked to stronger large-scale forcing as orographic forcing increases, leading to the development of precipitation at mid- to upper levels over a relatively large horizontal area that extends upstream of the coastal mountains. The ratio of average CZC rain rate to average BBY rain rate does not indicate a consistent functional relationship with orographic forcing. Values of this ratio increase from ~2 to 5 as upslope flow increases from ~0 to 20 m s^{-1} (Fig. 11a). In contrast, the ratio decreases as IWV increases (Fig. 11b). The relatively large ratio values at small IWV are due to average BBY rain-rate values near zero. Finally, ratio values meander from ~2 to 4 as IWV flux increases with no steady upward or downward trend.

b. *As a function of microphysics regime*

The impact of microphysics regime on the relationship between orographic forcing and orographic rain is explored by extracting the CZC BB rain and NBB rain populations from the 10-season composite. This CZC rain-type composite (hereafter referred to simply as the rain-type composite since CZC is the only site where rain-type information was derived and employed in this study) has significantly fewer samples than the overall composite due to criteria associated with application of the RPPA, particularly the requirement for rain rates in excess of 1 mm h^{-1}. The combination of the BB rain and NBB rain populations (hereafter referred to as BB+NBB) contains 1495 h of data (Table 2), which is ~37% of the data in the overall composite of 4058 h

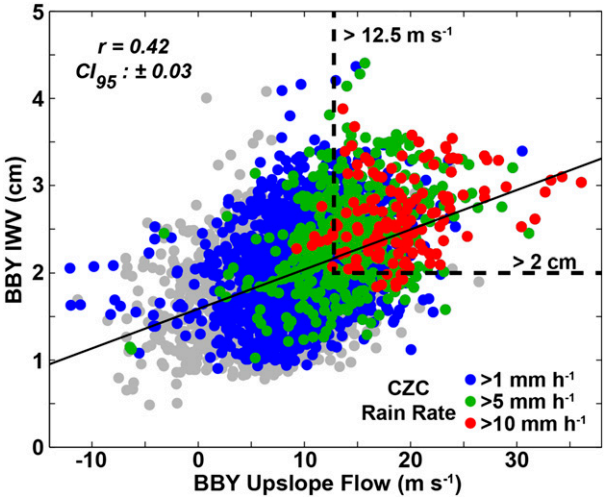

FIG. 9. Scatter of hourly upslope flow vs hourly IWV at BBY for the 10-season composite. The linear fit, correlation coefficient (i.e., r), and associated CI_{95} of the correlation coefficient are shown for each set of points. Points with CZC hourly rain rate exceeding 1, 5, and 10 mm h^{-1} are indicated by blue-, green-, and red-filled circles, respectively. Data are graphically presented in a manner similar to Fig. 8b of Neiman et al. (2009).

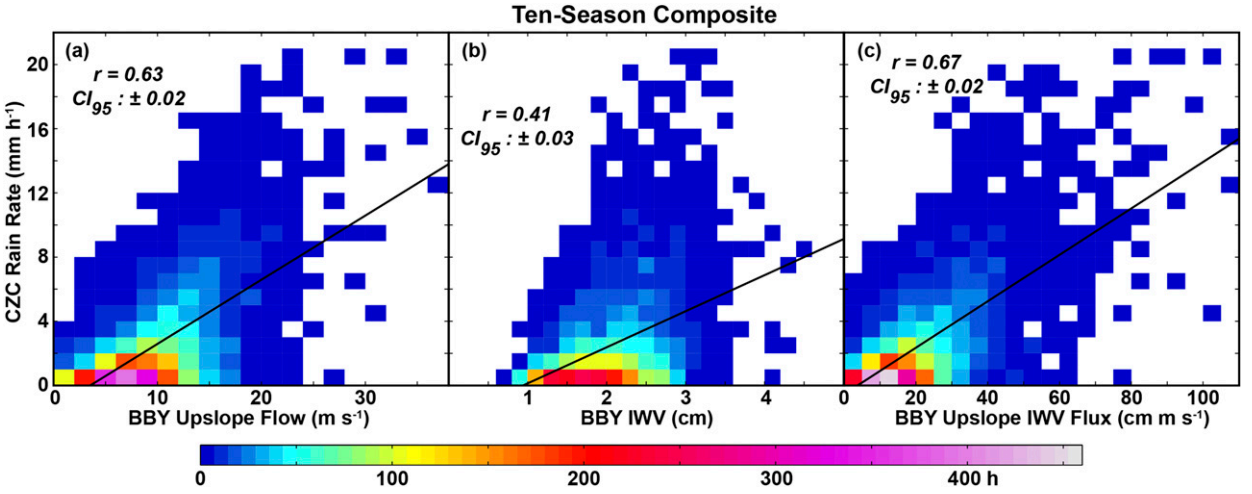

FIG. 10. Joint distributions of hourly (a) upslope flow (bins of 2 m s^{-1}), (b) IWV (bins of 0.2 cm), and (c) upslope IWV flux (bins of 5 cm m s^{-1}) at BBY vs hourly rain rate at CZC (bins of 1 mm h^{-1}) for the 10-season composite. Color scale at bottom indicates number of hours of data in each joint bin. The linear fit, correlation coefficient (i.e., r), and associated CI_{95} of the correlation coefficient of the unbinned scatter are shown for each set of parameters.

(Table 1). A total of 6584 mm of rain accumulated at CZC for the BB+NBB population in the rain-type composite. This equates to a mean rain rate of 4.4 mm h^{-1}, which is nearly double the 2.3 mm h^{-1} rate observed in the overall composite. Seasonal variations of CZC rainfall accumulations and mean rain rates in the rain-type composite mirrored the variations observed in the overall composite but with smaller accumulations (due to fewer hours of rainfall) and larger rates.

CZC rainfall accumulation in the rain-type composite is composed of 4435 mm BB rain and 2149 mm NBB rain, a fractional distribution of 67%–33% (Table 2). This fractional distribution varies from 53%–47% during 2006/07 to 85%–15% during 2001. These observations are consistent with those documented by White et al. (2003), Neiman et al. (2005), and White et al. (2015). The 10-season mean CZC rain rate associated with BB rain is 4.9 mm h^{-1}, about 33% larger than the rate of 3.7 mm h^{-1} observed for NBB rain. Seasonal mean rain rates of BB rain exceeded those for NBB rain in all seasons except 2004/05, when there were only 14 h of NBB rain.

The BB+NBB population of the rain-type composite is associated with 2230 mm of rainfall accumulation at BBY (Table 3). This accumulation occurs with about one-quarter of the 1495 hourly samples (360) having zero BBY rainfall. Similar to mean CZC rain rate, the mean BBY rain rate of 1.5 mm h^{-1} is about double the 0.8 mm h^{-1} BBY rain rate observed in the overall composite (see Table 1). BBY rainfall accumulation in the

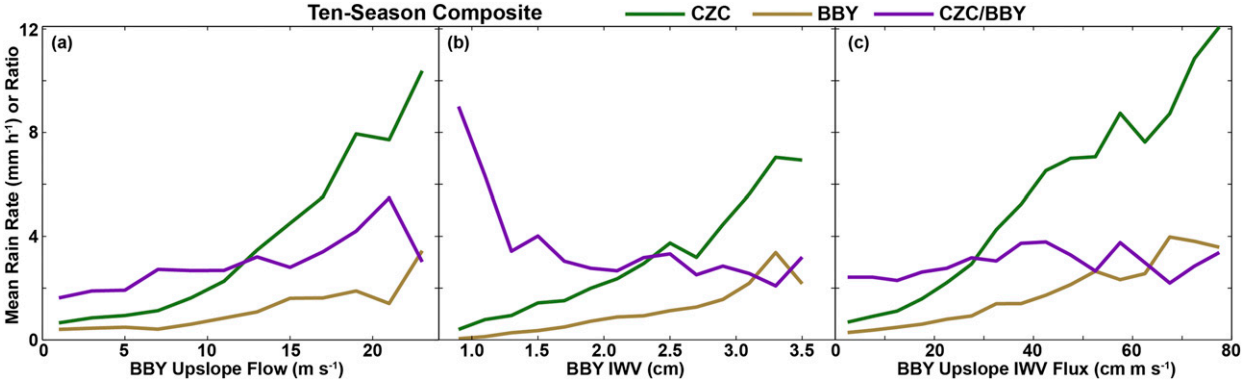

FIG. 11. Mean rain rate at CZC (green) and BBY (gold) in bins of hourly (a) upslope flow (bins of 2 m s^{-1}), (b) IWV (bins of 0.2 cm), and (c) upslope IWV flux (bins of 5 cm m s^{-1}) observed at BBY for the 10-season composite. Values are calculated for orographic-forcing bins having greater than 10 samples (Fig. 8). The ratio of mean rain rates at CZC and BBY is shown by the magenta lines.

TABLE 2. Rainfall characteristics at CZC for each of the 10 seasons in the CZC rain-type composite. Information is divided into separate sections for BB rain, NBB rain, and the combination of the two (BB+NBB). The 10-season totals for rain time and accumulation (Acc.) are shown at the bottom. Rain rates and accumulation fractions (Acc. frac.) in this row are based on total accumulations and rain time.

	BB+NBB			BB				NBB			
Season	Rain time (h)	Acc. (mm)	Rate (mm h^{-1})	Rain time (h)	Acc. (mm)	Acc. frac. (%)	Rate (mm h^{-1})	Rain time (h)	Acc. (mm)	Acc. frac. (%)	Rate (mm h^{-1})
2001	93	381	4.1	77	324	85	4.2	16	57	15	3.6
2003/04	104	545	5.2	50	328	60	6.6	54	217	40	4.0
2004/05	76	224	3.0	62	174	78	2.8	14	50	22	3.6
2005/06	265	1203	4.5	157	786	65	5.0	108	417	35	3.9
2006/07	141	609	4.3	65	324	53	5.0	76	285	47	3.8
2007/08	150	853	5.7	93	610	72	6.6	57	243	28	4.3
2008/09	169	582	3.4	94	350	60	3.7	75	232	40	3.1
2009/10	217	1000	4.6	135	717	72	5.3	82	283	28	3.5
2010/11	159	690	4.3	105	469	68	4.5	54	221	32	4.1
2011/12	121	497	4.1	72	353	71	4.9	49	144	29	2.9
Total	1495	6584	4.4	910	4435	67	4.9	585	2149	33	3.7

rain-type composite is composed of 1653 mm BB rain and 577 mm NBB rain, a fractional distribution of 74%–26%. The 10-season mean BBY rain rate associated with CZC BB rain is 1.8 mm h^{-1}, 80% larger than the rate of 1.0 mm h^{-1} observed for CZC NBB rain.

The rainfall ratio between CZC and BBY in the BB+NBB population of the 10-season rain-type composite is 3.0 (Table 4), which is about the same as observed for the overall composite (see Table 1). Ratios were larger during NBB rain compared to BB rain, a result consistent with the findings of White et al. (2003) and indicative of the relative importance of orographic enhancement during NBB conditions. Seasonal variations of CZC/BBY rainfall ratio for the BB+NBB population are closely correlated to those for the overall composite. The range of ratio variation is larger for NBB rain compared to BB rain.

The distribution of hourly rain rates at CZC and BBY for the rain-type composite (Fig. 12) is generally similar to the overall composite (Fig. 7). Specifically, the distribution of rain rates at BBY is narrower than at CZC. A notable difference is the lack of CZC rain rates below 1 mm h^{-1} due to application of the RPPA at CZC. The distribution of rain rates at both sites is narrower for NBB rain compared to BB rain.

Mean values of orographic forcing in the rain-type composite (Fig. 13) are larger than those in the overall composite (Fig. 8). Upslope flow in the BB+NBB population has a μ of 11.7 m s^{-1} (Fig. 13a), 30% larger than the μ of upslope flow in the overall composite. Mean IWV in the BB+NBB population (Fig. 13b) is also larger than in the overall composite, but only by 15%. IWV flux in the BB+NBB population (Fig. 13c) exhibits the largest increase relative to the overall

TABLE 3. Rainfall characteristics at BBY for each of the 10 seasons in the CZC rain-type composite. Information is divided into separate sections for BB rain, NBB rain, and the combination of the two (BB+NBB). Rain rates at BBY are based on rain time at CZC; no-rain time at BBY represents the subset of CZC rain time when no rain is observed at BBY. The 10-season totals for rain time and accumulation (Acc.) are shown at the bottom. Rain rates and accumulation fractions (Acc. frac.) in this row are based on total accumulations and rain time.

	BB+NBB			BB				NBB			
Season	(No-rain time) Rain time (h)	Acc. (mm)	Rate (mm h^{-1})	(No-rain time) Rain time (h)	Acc. (mm)	Acc. frac. (%)	Rate (mm h^{-1})	(No-rain time) Rain time (h)	Acc. (mm)	Acc. frac. (%)	Rate (mm h^{-1})
2001	(22) 93	144	1.6	(18) 77	125	87	1.6	(4) 16	19	13	1.2
2003/04	(16) 104	237	2.3	(4) 50	172	73	3.4	(12) 54	65	27	1.2
2004/05	(6) 76	161	2.1	(4) 62	120	75	1.9	(2) 14	41	25	2.9
2005/06	(50) 265	480	1.8	(29) 157	325	68	2.1	(21) 108	155	32	1.4
2006/07	(27) 141	202	1.4	(5) 65	132	65	2.0	(22) 76	70	35	0.9
2007/08	(46) 150	208	1.4	(14) 93	169	81	1.8	(32) 57	39	19	0.7
2008/09	(69) 169	118	0.7	(26) 94	86	73	0.9	(43) 75	32	27	0.4
2009/10	(64) 217	258	1.2	(30) 135	206	80	1.5	(34) 82	52	20	0.6
2010/11	(35) 159	277	1.7	(20) 105	217	78	2.1	(15) 54	60	22	1.1
2011/12	(25) 121	145	1.2	(7) 72	101	70	1.4	(18) 49	44	30	0.9
Total	(360) 1495	2230	1.5	(157) 910	1653	74	1.8	(203) 585	577	26	1.0

TABLE 4. Ratio of CZC rain rate divided by BBY rain rate for each of the 10 seasons in the CZC rain-type composite. Information is divided into separate columns for BB rain, NBB rain, and the combination of the two (BB+NBB). The 10-season totals at the bottom are based on CZC and BBY rain rates at the bottom of Tables 2 and 3, respectively.

Season	BB+NBB	BB	NBB
2001	2.7	2.6	3.0
2003/04	2.3	1.9	3.3
2004/05	1.4	1.5	1.2
2005/06	2.5	2.4	2.7
2006/07	3.0	2.5	4.1
2007/08	4.1	3.6	6.2
2008/09	4.9	4.1	7.3
2009/10	3.9	3.5	5.4
2010/11	2.5	2.2	3.7
2011/12	3.4	3.5	3.3
Total	3.0	2.7	3.7

composite (~43%) with a μ of 27.7 cm m s^{-1}. The differences in mean orographic forcing between the BB+NBB population and the overall composite are significant at the 95% confidence level. NBB rain has noticeably larger mean values of upslope flow and IWV flux compared to BB rain, the former by 16% and the latter by 19%. Mean IWV is also larger for NBB rain compared to BB rain, but the difference is relatively minor. Nonetheless, the difference is significant at the 95% confidence level.

The scatter of upslope flow versus IWV in the BB+NBB population (Fig. 14a) has r of 0.38, which is slightly smaller than the r of 0.42 observed for the overall composite (Fig. 9), a difference that is not significant at the 95% confidence level. These two parameters are better correlated for BB rain (r = 0.40, Fig. 14b) than NBB rain (r = 0.30, Fig. 14c), but this difference is also not significant at the 95% confidence level. There is a tendency for larger CZC rain rates as upslope flow and IWV increase, a trend also observed in the overall composite. Rain rates exceeding 10 mm h^{-1} occurred 89%, 88%, and 92% of the time when upslope flow exceeded 12.5 m s^{-1} and IWV exceeded 2 cm (i.e., AR conditions) for the BB+NBB, BB, and NBB populations, respectively. Corresponding false alarm ratios for these populations were 81%, 73%, and 90%, respectively. These percentages are similar to the overall composite. For BB rain, the 10 mm h^{-1} exceedances extended up to 36.1 m s^{-1} of upslope flow and up to 3.9 cm of IWV. Exceedances for NBB rain extended up to similar values of upslope flow (34.3 m s^{-1}) but only up to 3.1 cm of IWV.

The joint distribution of CZC rain rate versus BBY orographic forcing for the rain-type composite provides an alternative illustration of the relationship (Fig. 15).

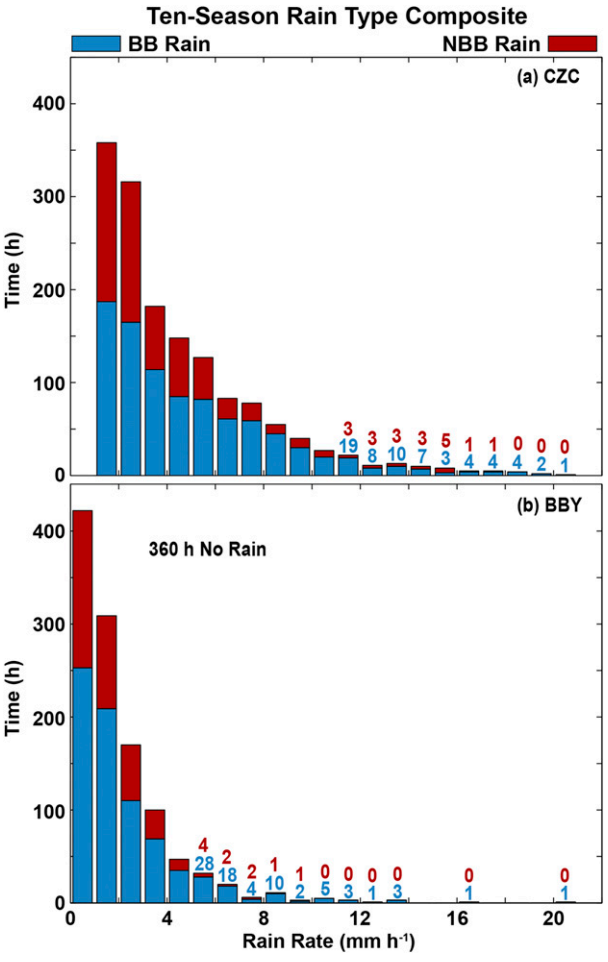

FIG. 12. Stacked histograms of hourly rain rate at (a) CZC and (b) BBY for the 10-season rain-type composite. Upper (lower) portions of the bars in red (blue) correspond to NBB (BB) rain. Rain-rate bins of 1 mm h^{-1} are used. The number of hours is shown above bars having less than 5 h of NBB or BB data. Upper (lower) numbers in red (blue) correspond to NBB (BB) rain.

Correlation of these parameters is smaller in the BB+NBB population (Figs. 15a–c) compared to the overall composite, especially for IWV and IWV flux where the reductions in correlation coefficient are significant at the 95% confidence level. It is notable that r for IWV flux (0.59) is not larger than that for upslope flow (0.61), which is in contrast to the overall composite and to the results of Neiman et al. (2009). Correlation coefficients of rain rate versus orographic forcing are smaller for NBB rain (Figs. 15g–i) compared to BB rain (Figs. 15d–f), with the largest contrast evident for IWV. However, these differences are not significant at the 95% confidence level. Except for the unbinned scatter associated with NBB IWV, the BB and NBB correlation coefficients are slightly larger than correlation coefficients for the BB+NBB population. Again, however,

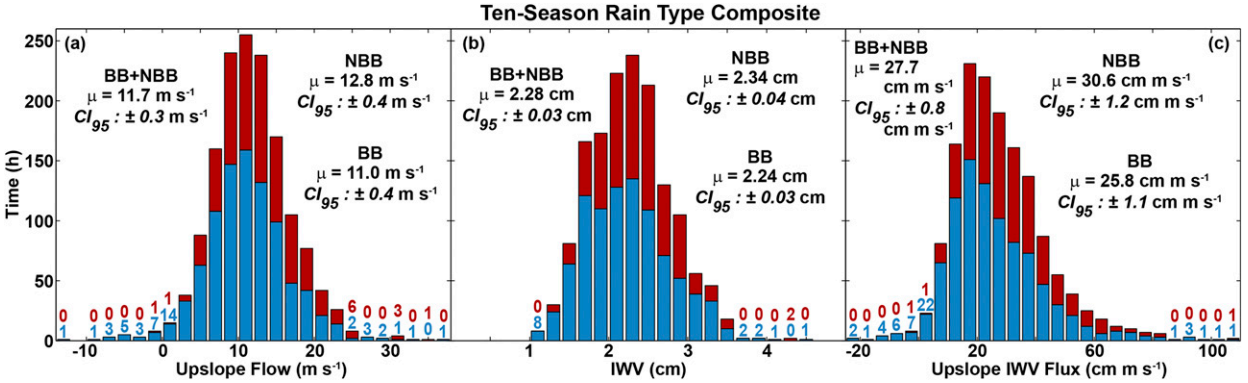

FIG. 13. Stacked histograms of hourly (a) upslope flow (bins of 2 m s^{-1}), (b) IWV (bins of 0.2 cm), and (c) upslope IWV flux (bins of 5 cm m s^{-1}) at BBY for the 10-season rain-type composite. Upper (lower) portions of the bars in red (blue) correspond to NBB (BB) rain. The mean (i.e., μ) and associated CI_{95} of the mean for each distribution are indicated separately for BB rain, NBB rain, and their combination (BB+NBB). The number of hours is shown above bars having less than 3 h of NBB or BB data. Upper (lower) numbers in red (blue) correspond to NBB (BB) rain.

these differences are not significant at the 95% confidence level.

Over the range of observed orographic forcing in the BB+NBB population, average CZC rain rate increases the least with IWV (Figs. 16a–c), which is consistent with the overall composite (Fig. 11). CZC rain rate increases more as a function of orographic forcing for BB rain (Figs. 16d–f) than NBB rain (Figs. 16g–i). Alternately stated, CZC rain rates are larger for BB rain compared to NBB rain for a given amount of orographic forcing. Ice particles aloft are available in BB rain to seed the low-level orographic feeder cloud and enhance rainfall relative to NBB rain where the orographic feeder cloud must produce precipitation via the warm-rain process without assistance from seeder particles aloft.

Average BBY rain rate from the BB+NBB population increases as orographic forcing increases in much the same way as the overall composite. The amount of increase is slightly larger for BB rain compared to NBB rain, suggesting that the seeder clouds enhancing precipitation over CZC during BB rain extend over a large enough area to be enhancing precipitation over BBY. Ratios of average CZC rain rate to average BBY rain rate in the BB+NBB population exhibit similar trends with respect to orographic forcing as those observed in the overall composite. Trends in ratio as a function of forcing become less clear when discriminating by rain type. The only clear difference is generally larger values of ratio for NBB rain compared to BB rain, which is consistent with the results shown in Table 4.

5. Summary and conclusions

This study has explored the impact of microphysics regime on the relationship between orographic forcing

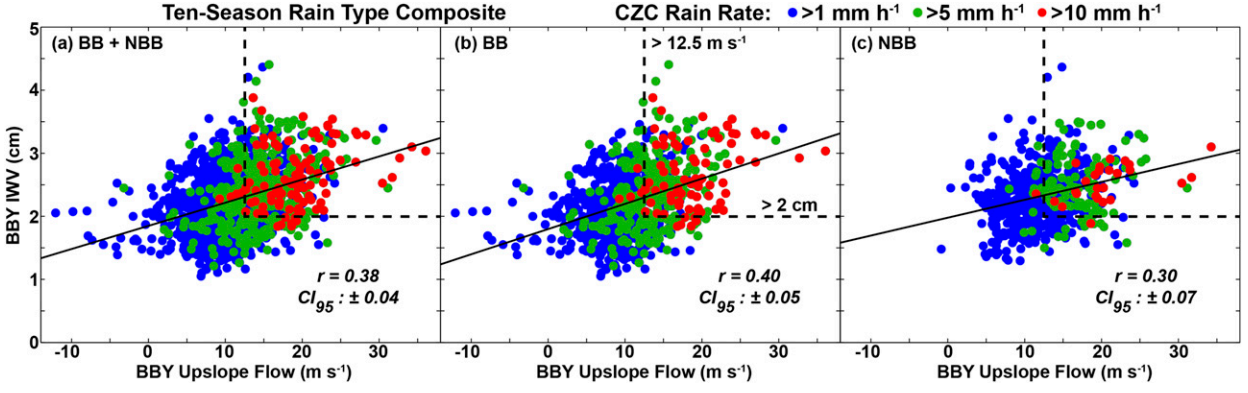

FIG. 14. Scatter of hourly upslope flow vs hourly IWV at BBY for the 10-season rain-type composite: (a) BB+NBB, (b) BB, and (c) NBB rain. The linear fit, correlation coefficient (i.e., r), and associated CI_{95} of the correlation coefficient are shown for each set of points. Points with CZC hourly rain rate exceeding 1, 5, and 10 mm h^{-1} are indicated by blue-, green-, and red-filled circles, respectively. Data are graphically presented in a manner similar to Fig. 8b of Neiman et al. (2009).

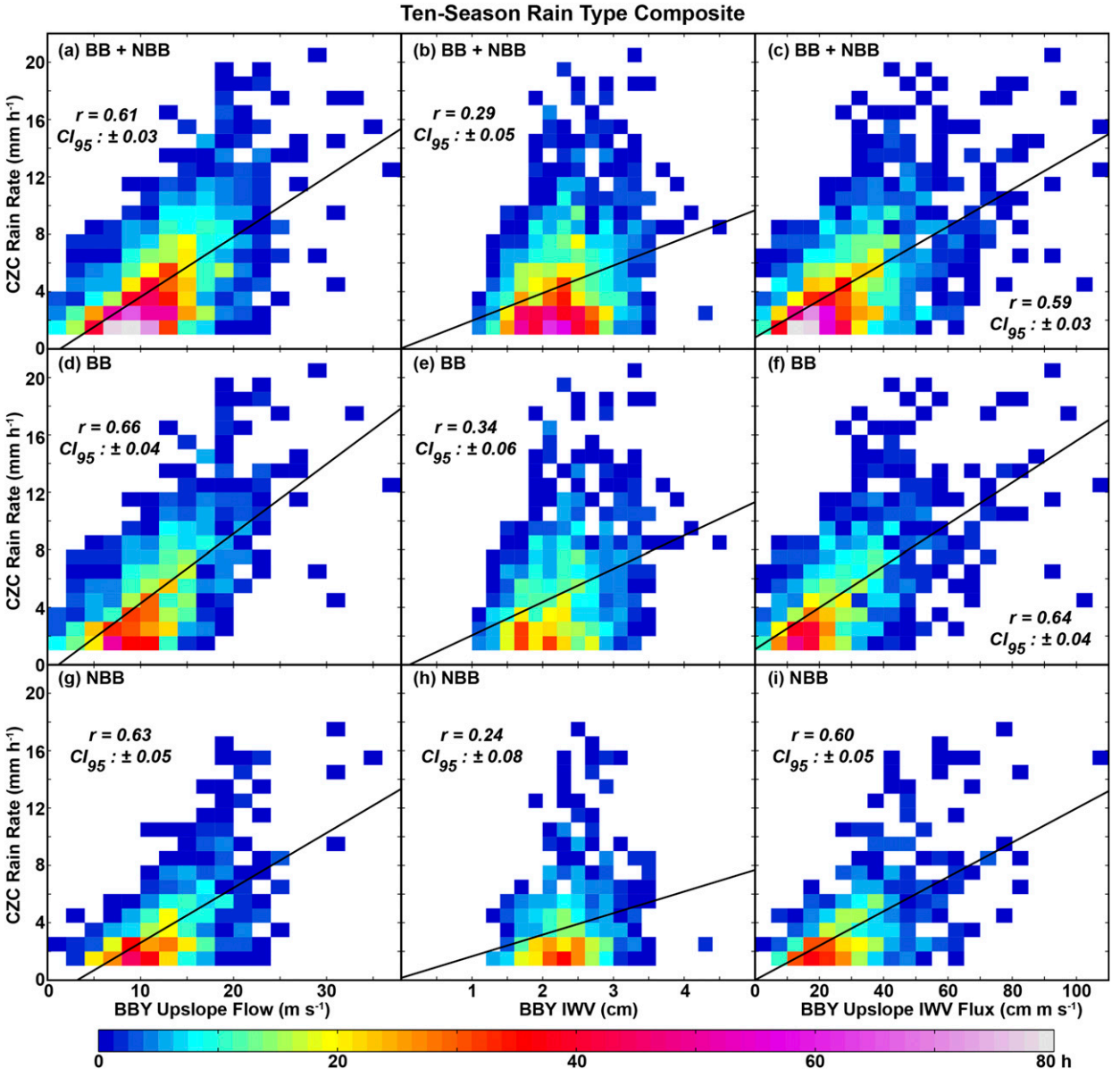

FIG. 15. Joint distributions of hourly (left) upslope flow (bins of 2 m s^{-1}), (center) IWV (bins of 0.2 cm), and (right) upslope IWV flux (bins of 5 cm m s^{-1}) at BBY vs hourly rain rate at CZC (bins of 1 mm h^{-1}) for the 10-season rain-type composite: (a)–(c) BB+NBB, (d)–(f) BB, and (g)–(i) NBB rain. Color scale at bottom indicates number of hours of data in each joint bin. The linear fit, correlation coefficient (i.e., r), and associated CI_{95} of the correlation coefficient of the unbinned scatter are shown for each set of parameters.

and orographic rain in the coastal mountains of Northern California using data from profiling Doppler radars, rain gauges, and a GPS receiver collected over 10 cool seasons. Forcing was documented by hourly upslope flow, IWV, and IWV flux derived from a wind profiler and GPS receiver located along the coast at BBY. Microphysics regime was inferred by examining data from a vertically pointing precipitation profiler in the coastal mountains at CZC, which allowed designation of hourly periods dominated by the seeder–feeder process (BB rain) or the warm-rain process (NBB rain). Rain accumulations and rates at both sites were characterized with tipping-bucket gauge data.

The relationship between orographic forcing and orographic rain was first documented independent of microphysics regime. Rain rate at CZC increased as orographic forcing at BBY increased. The correlation coefficients for CZC rain rate versus BBY upslope flow, IWV, and IWV flux were 0.63, 0.41, and 0.67, respectively (Fig. 10). While the correlation of CZC rain rate

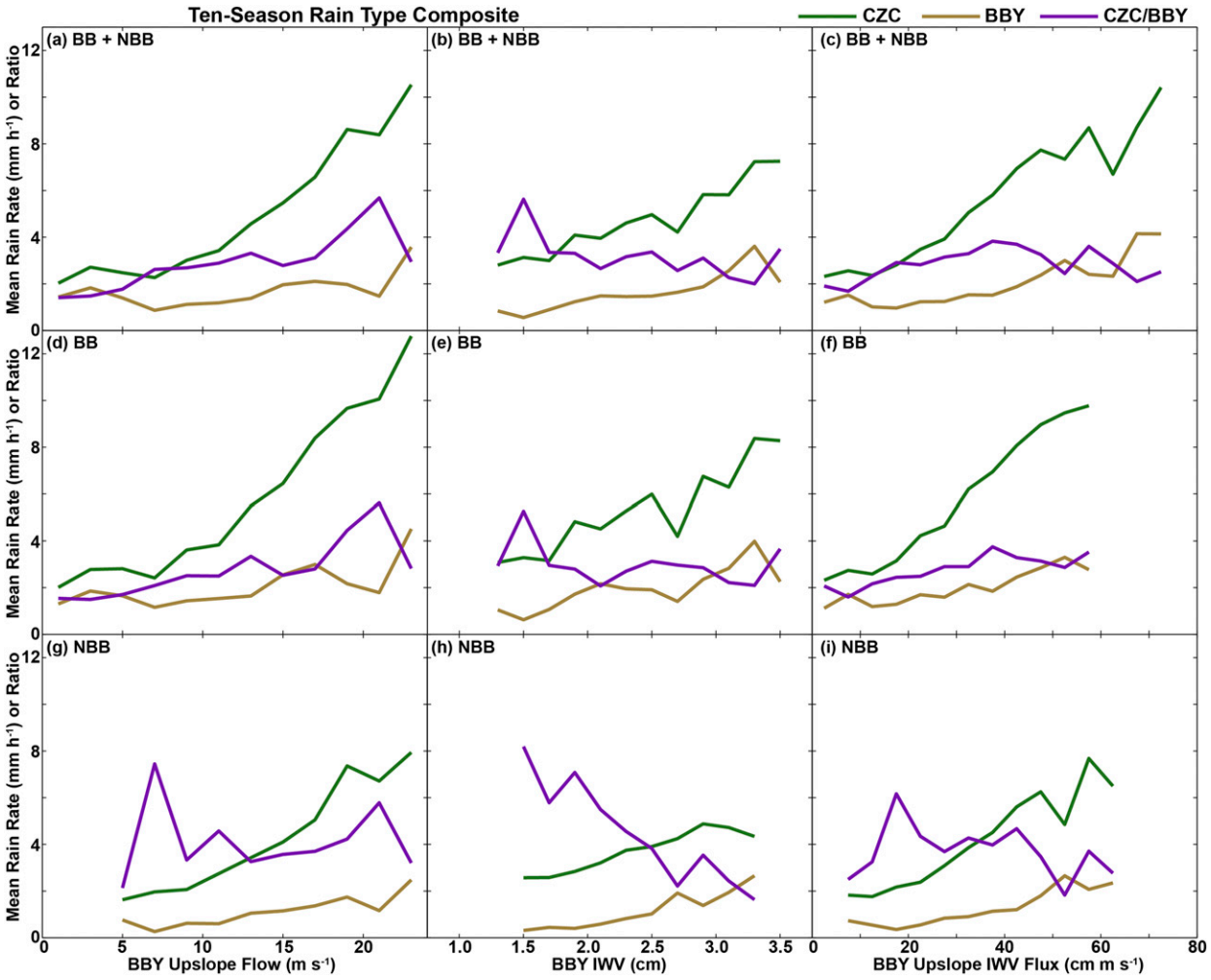

FIG. 16. Mean rain rate at CZC (green) and BBY (gold) in bins of hourly (left) upslope flow (bins of 2 m s^{-1}), (center) IWV (bins of 0.2 cm), and (right) upslope IWV flux (bins of 5 cm m s^{-1}) observed at BBY for the 10-season rain-type composite: (a)–(c) BB+NBB, (d)–(f) BB, and (g)–(i) NBB rain. Values are calculated for orographic-forcing bins having greater than 10 samples (Fig. 13). The ratio of mean rain rates at CZC and BBY is shown by the magenta lines.

with IWV was relatively poor, the correlation with the product of IWV and upslope flow (i.e., IWV flux) was improved in a statistically significant sense relative to that with upslope flow alone. These results are generally consistent with those reported by Neiman et al. (2009).

A rain-type composite was derived by extracting the BB and NBB rain populations from the overall composite to examine the impact of microphysics regime on the relationship between orographic forcing and orographic rain. BB and NBB rain accounted for 67% and 33% of the total CZC rain accumulation, respectively, which is consistent with the multiseason results reported by Neiman et al. (2005) and White et al. (2015). NBB rain was associated with larger mean values of orographic forcing compared to BB rain. The relationship between orographic forcing at BBY and orographic rain at CZC in the rain-type composite had smaller correlation coefficients (Fig. 15) than observed in the overall composite. These differences were significant at the 95% confidence level for IWV and IWV flux, but not for upslope flow. Additionally, correlation coefficients for IWV flux were not statistically distinct from those for upslope flow, which also differs from the overall composite and from Neiman et al. (2009). NBB rain was associated with smaller correlation coefficients compared to BB rain, but these differences were not significant at the 95% confidence level. CZC rain rates were larger for BB rain compared to NBB rain for a given amount of orographic forcing (Fig. 16).

While the results from this study show some similarities with those from Neiman et al. (2009), they also raise some questions. For example, why is the relationship

between orographic forcing at BBY and orographic rainfall at CZC degraded from a correlation coefficient standpoint in the rain-type composite relative to the overall composite? Also, why does GPS-derived IWV information improve the relationship in the overall composite but provide no benefit in the rain-type composite? The rain-type composite primarily differs from the overall composite in that it excludes samples with CZC rain rates less than 1 mm h^{-1}. This implies that the correlation coefficients in the overall composite owe their larger values to samples with rain rates less than 1 mm h^{-1}, which suggests that the relationship between orographic forcing and orographic rainfall becomes less correlated and the influence of IWV information diminishes as rain rate increases. One ramification of this result is that it raises concerns about applying the relationship to hydrologically sensitive rainfall events. Additionally, it casts doubt regarding the value of GPS-derived IWV information in documenting orographic forcing for the purpose of diagnosing orographic rainfall.

Another relevant reference for comparison to this study is White et al. (2003), who employed a slightly different analysis approach to a much smaller dataset. Their overall composite contained 602 h of data derived from 33 significant precipitation events observed at CZC during a single cool season. Also, White et al. (2003) only examined the 38-h NBB rain subset of their 33-event composite and used a more stringent threshold to define NBB rain (i.e., less than 20% of the S-PROF profiles within an hour could contain a bright band as opposed to the 50% threshold in the present study). Finally, they characterized orographic forcing at CZC instead of BBY and only used upslope flow since GPS IWV information was not available at the time. Despite these differences, it is informative to compare the results of the present study with White et al. (2003).

Mean CZC rain rates for NBB rain and the overall composite of the present study were smaller than White et al. (2003) by ~25% (3.7 and 2.3 mm h^{-1}, respectively), but had a similar relative ratio of ~1.6. The ratio of mean rain rate at CZC and BBY in the present study was 3.7 and 2.9 for NBB rain and the overall composite, respectively, which slightly differs from the corresponding values of 4.0 and 2.2 in White et al. (2003). Mean upslope flow above BBY in the present study was 42% larger for NBB rain compared to the overall composite, which is similar to the 30% relative increase of these variables observed by White et al. (2003), even though they measured mean upslope flow above CZC. The most dramatic difference in results from the two studies is in the correlation between upslope flow and CZC rain rate. White et al. (2003) found that the correlation coefficient between these parameters was 0.74 for NBB rain but only 0.52 for their 33-event composite. In contrast, the corresponding correlation coefficients in the present study were both 0.63. One possible explanation for the difference is that upslope flow was derived at different locations separated by ~35 km in the two studies. Probably a more likely explanation is the significantly larger dataset associated with the present study compared to White et al. (2003).

At the outset of this paper it was asserted that cloud and precipitation microphysics was perhaps the largest source of uncertainty in the relationship between orographic forcing and orographic rainfall. The results of this study provide evidence to reject this hypothesis. While correlation coefficients for the microphysically distinct BB and NBB populations were slightly larger than those for the BB+NBB population, the differences were not statistically significant. However, the two microphysics regimes employed in this study were limited in that they were derived from precipitation profiler data, which does not allow a comprehensive characterization of all microphysical processes active in development of coastal orographic rainfall. Thus, it may be premature to reject the hypothesis altogether. Future studies should attempt to address the problem with more detailed microphysics information, including in situ observations. They also should examine other possible sources of uncertainty, such as large-scale forcing, transient mesoscale features (e.g., fronts and jet streaks), and terrain-trapped airflows (Neiman et al. 2002; Valenzuela and Kingsmill 2015). Finally, future studies should employ numerical weather prediction models to evaluate the various uncertainties in the relationship through a sensitivity-study approach.

Acknowledgments. The authors thank the NOAA/ESRL observing systems team for deploying and operating the instrumentation whose data were employed in this study. Tim Coleman of CIRES/ESRL processed and quality controlled the wind profiler, GPS-IWV, surface meteorology, and rain gauge data. We appreciate the comments and suggestions of Dave Reynolds of CIRES/ESRL and two anonymous reviewers on earlier versions of this manuscript. This research was sponsored by the National Science Foundation under Grant AGS-1144271 and supported the efforts of David Kingsmill.

REFERENCES

Bergeron, T., 1965: On the low-level redistribution of atmospheric water caused by orography. *Proc. Int. Conf. on Cloud Physics*, Tokyo, Japan, IAMAP/WMO, 96–100.

Browning, K. A., 1980: Structure, mechanism, and prediction of orographically enhanced rain in Britain. *Orographic Effects in*

Planetary Flows, R. Hide and P. W. White, Eds., GARP Publication Series, Vol. 23, WMO, 85–114.

Carter, D. A., K. S. Gage, W. L. Ecklund, W. M. Angevine, P. E. Johnston, A. C. Riddle, J. Wilson, and C. R. Williams, 1995: Developments in UHF lower tropospheric wind profiling at NOAA's Aeronomy Laboratory. *Radio Sci.*, **30**, 977–1001, doi:10.1029/95RS00649.

Collier, C. G., 1975: A representation of the effects of topography on surface rainfall within moving baroclinic disturbances. *Quart. J. Roy. Meteor. Soc.*, **101**, 407–422, doi:10.1002/qj.49710142902.

Dettinger, M. D., K. Redmond, and D. Cayan, 2004: Winter orographic precipitation ratios in the Sierra Nevada—Large-scale atmospheric circulations and hydrologic consequences. *J. Hydrometeor.*, **5**, 1102–1116, doi:10.1175/JHM-390.1.

Duan, J. M., and Coauthors, 1996: GPS meteorology: Direct estimation of the absolute value of precipitable water. *J. Appl. Meteor.*, **35**, 830–838, doi:10.1175/1520-0450(1996)035<0830:GMDEOT>2.0.CO;2.

Ecklund, W. L., D. A. Carter, and B. B. Balsley, 1988: A UHF wind profiler for the boundary layer: Brief description and initial results. *J. Atmos. Oceanic Technol.*, **5**, 432–441, doi:10.1175/1520-0426(1988)005<0432:AUWPFT>2.0.CO;2.

Elliott, R. D., and E. L. Hovind, 1964: The water balance of orographic clouds. *J. Appl. Meteor.*, **3**, 235–239, doi:10.1175/1520-0450(1964)003<0235:TWBOOC>2.0.CO;2.

Hill, F. F., K. A. Browning, and M. J. Bader, 1981: Radar and rain gauge observations of orographic rain over south Wales. *Quart. J. Roy. Meteor. Soc.*, **107**, 643–670, doi:10.1002/qj.49710745312.

Hobbs, P. V., 1975: The nature of winter clouds and precipitation in the Cascade Mountains and their modification by artificial seeding. Part I: Natural conditions. *J. Appl. Meteor.*, **14**, 783–804, doi:10.1175/1520-0450(1975)014<0783:TNOWCA>2.0.CO;2.

Kingsmill, D. E., P. J. Neiman, F. M. Ralph, and A. B. White, 2006: Synoptic and topographic variability of Northern California precipitation characteristics in landfalling winter storms observed during CALJET. *Mon. Wea. Rev.*, **134**, 2072–2094, doi:10.1175/MWR3166.1.

——, ——, B. J. Moore, M. Hughes, S. E. Yuter, and F. M. Ralph, 2013: Kinematic and thermodynamic structures of Sierra barrier jets and overrunning atmospheric rivers during a landfalling winter storm in Northern California. *Mon. Wea. Rev.*, **141**, 2015–2036, doi:10.1175/MWR-D-12-00277.1.

Martner, B. E., S. E. Yuter, A. B. White, S. Y. Matrosov, D. E. Kingsmill, and F. M. Ralph, 2008: Raindrop size distributions and rain characteristics in California coastal rainfall for periods with and without a radar bright band. *J. Hydrometeor.*, **9**, 408–425, doi:10.1175/2007JHM924.1.

Mattioli, V., E. R. Westwater, C. Cimini, J. S. Liljegren, B. M. Lesht, S. I. Gutman, and F. J. Schmidlin, 2007: Analysis of radiosonde and ground-based remotely sensed PWV data from the 2004 North Slope of Alaska Arctic Winter Radiometric Experiment. *J. Atmos. Oceanic Technol.*, **24**, 415–431, doi:10.1175/JTECH1982.1.

Medina, S., E. Sukovich, and R. A. Houze Jr., 2007: Vertical structures of precipitation in cyclones crossing the Oregon Cascades. *Mon. Wea. Rev.*, **135**, 3565–3586, doi:10.1175/MWR3470.1.

Neiman, P. J., F. M. Ralph, A. B. White, D. E. Kingsmill, and P. O. G. Persson, 2002: The statistical relationship between upslope flow and rainfall in California's coastal mountains: Observations during CALJET. *Mon. Wea. Rev.*, **130**, 1468–1492, doi:10.1175/1520-0493(2002)130<1468:TSRBUF>2.0.CO;2.

——, G. A. Wick, F. M. Ralph, B. E. Martner, A. B. White, and D. E. Kingsmill, 2005: Wintertime nonbrightband rain in California and Oregon during CALJET and PACJET: Geographic, interannual, and synoptic variability. *Mon. Wea. Rev.*, **133**, 1199–1223, doi:10.1175/MWR2919.1.

——, A. B. White, F. M. Ralph, D. J. Gottas, and S. I. Gutman, 2009: A water vapour flux tool for precipitation forecasting. *Proc. Inst. Civ. Eng. Water Manage.*, **162**, 83–94, doi:10.1680/wama.2009.162.2.83.

——, M. Hughes, B. J. Moore, F. M. Ralph, and E. S. Sukovich, 2013: Sierra barrier jets, atmospheric rivers, and precipitation characteristics in Northern California: A composite perspective based on a network of wind profilers. *Mon. Wea. Rev.*, **141**, 4211–4233, doi:10.1175/MWR-D-13-00112.1.

NOAA, 1982: *Storm Data*. Vol. 24, No. 3, NOAA, Silver Spring, MD, 31 pp. [Available online at http://www.ncdc.noaa.gov/IPS/sd/sd.html.]

——, 1998: *Storm Data*. Vol. 40, No. 2, NOAA, Silver Spring, MD, 183 pp. [Available online at http://www.ncdc.noaa.gov/IPS/sd/sd.html.]

Nordø, J., and K. Hjortnæs, 1966: Statistical studies of precipitation on local, national, and continental scales. *Geofys. Publ.*, **26**, 1–46.

Ralph, F. M., P. J. Neiman, D. E. Kingsmill, P. O. G. Persson, A. B. White, E. T. Strem, E. D. Andrews, and R. C. Antweiler, 2003: The impact of a prominent rain shadow on flooding in California's Santa Cruz Mountains: A CALJET case study and sensitivity to the ENSO cycle. *J. Hydrometeor.*, **4**, 1243–1264, doi:10.1175/1525-7541(2003)004<1243:TIOAPR>2.0.CO;2.

——, ——, and G. A. Wick, 2004: Satellite and CALJET aircraft observations of atmospheric rivers over the eastern North Pacific Ocean during the winter of 1997/98. *Mon. Wea. Rev.*, **132**, 1721–1745, doi:10.1175/1520-0493(2004)132<1721:SACAOO>2.0.CO;2.

——, ——, and R. Rotunno, 2005: Dropsonde observations in low-level jets over the northeastern Pacific Ocean from CALJET-1998 and PACJET-2001: Mean vertical-profile and atmospheric-river characteristics. *Mon. Wea. Rev.*, **133**, 889–910, doi:10.1175/MWR2896.1.

——, and Coauthors, 2013a: The emergence of weather-related testbeds linking research and forecasting operations. *Bull. Amer. Meteor. Soc.*, **94**, 1187–1211, doi:10.1175/BAMS-D-12-00080.1.

——, T. Coleman, P. J. Neiman, R. J. Zamora, and M. D. Dettinger, 2013b: Observed impacts of duration and seasonality of atmospheric-river landfalls on soil moisture and runoff in coastal Northern California. *J. Hydrometeor.*, **14**, 443–459, doi:10.1175/JHM-D-12-076.1.

Reynolds, D. W., and A. S. Dennis, 1986: A review of the Sierra Cooperative Pilot Project. *Bull. Amer. Meteor. Soc.*, **67**, 513–523, doi:10.1175/1520-0477(1986)067<0513:AROTSC>2.0.CO;2.

Rhea, J. O., 1978: Orographic precipitation model for hydrometeorological use. Ph.D. dissertation, Department of Atmospheric Science Paper 287, Colorado State University, Fort Collins, CO, 198 pp.

Sinclair, M. R., 1994: A diagnostic model for estimating orographic precipitation. *J. Appl. Meteor.*, **33**, 1163–1175, doi:10.1175/1520-0450(1994)033<1163:ADMFEO>2.0.CO;2.

Smith, P. L., and Coauthors, 2005: *Flash Flood Forecasting over Complex Terrain: With an Assessment of the Sulphur Mountain NEXRAD in Southern California*. National Academies Press, 191 pp., doi:10.17226/11128.

Stoelinga, M. T., and Coauthors, 2003: Improvement of Microphysical Parameterization through Observational Verification

Experiment (IMPROVE). *Bull. Amer. Meteor. Soc.*, **84**, 1807–1826, doi:10.1175/BAMS-84-12-1807.

Valenzuela, R. A., and D. E. Kingsmill, 2015: Orographic precipitation forcing along the coast of Northern California during a landfalling winter storm. *Mon. Wea. Rev.*, **143**, 3570–3590, doi:10.1175/MWR-D-14-00365.1.

Weber, B. L., D. B. Wuertz, D. C. Welsh, and R. McPeek, 1993: Quality controls for profiler measurements of winds and RASS temperatures. *J. Atmos. Oceanic Technol.*, **10**, 452–464, doi:10.1175/1520-0426(1993)010<0452:QCFPMO>2.0.CO;2.

White, A. B., J. R. Jordan, B. E. Martner, F. M. Ralph, and B. W. Bartram, 2000: Extending the dynamic range of an S-band radar for cloud and precipitation studies. *J. Atmos. Oceanic Technol.*, **17**, 1226–1234, doi:10.1175/1520-0426(2000)017<1226:ETDROA>2.0.CO;2.

——, D. J. Gottas, E. Strem, F. M. Ralph, and P. J. Neiman, 2002: An automated brightband height detection algorithm for use with Doppler radar spectral moments. *J. Atmos. Oceanic Technol.*, **19**, 687–697, doi:10.1175/1520-0426(2002)019<0687:AABHDA>2.0.CO;2.

——, P. J. Neiman, F. M. Ralph, D. E. Kingsmill, and P. O. G. Persson, 2003: Coastal orographic rainfall processes observed by radar during the California Land-Falling Jets Experiment. *J. Hydrometeor.*, **4**, 264–282, doi:10.1175/1525-7541(2003)4<264:CORPOB>2.0.CO;2.

——, ——, J. M. Creamean, T. Coleman, F. M. Ralph, and K. A. Prather, 2015: The impacts of California's San Francisco Bay area gap on precipitation observed in the Sierra Nevada during HMT and CalWater. *J. Hydrometeor.*, **16**, 1048–1069, doi:10.1175/JHM-D-14-0160.1.

Zhu, Y., and R. E. Newell, 1998: A proposed algorithm for moisture fluxes from atmospheric rivers. *Mon. Wea. Rev.*, **126**, 725–735, doi:10.1175/1520-0493(1998)126<0725:APAFMF>2.0.CO;2.